Journal of Neurology (2019) 266:3087–3097
https://doi.org/10.1007/s00415-019-09530-7

ORIGINAL COMMUNICATION

[^{18}F]-AV-1451 tau PET imaging in Alzheimer's disease and suspected non-AD tauopathies using a late acquisition time window

Julien Lagarde[1,2] · Pauline Olivieri[1] · Fabien Caillé[2] · Philippe Gervais[2] · Jean-Claude Baron[3] · Michel Bottlaender[2,4] · Marie Sarazin[1,2]

Received: 7 April 2019 / Revised: 4 September 2019 / Accepted: 6 September 2019 / Published online: 18 September 2019

Abstract

The utility of tau PET imaging in non-Alzheimer's disease (AD) tauopathies like behavioural frontotemporal dementia (bvFTD), which is mainly underlain by TDP-43 or tau pathology, remains debated. We aim to test the hypothesis that [^{18}F]-AV-1451 tau PET using later than usual acquisition times, which have previously been shown in AD to allow to get closer to tracer equilibrium between the reference region and high-binding structures, and could be better suited to the lower affinity of this tracer for the straight tau filaments present in non-AD tauopathies, would allow to detect cortical tau pathology in a fraction of bvFTD patients and in patients with non-fluent primary progressive aphasia (nfPPA, most often underlain by tau pathology). Sixteen AD patients, 11 controls, 7 bvFTD patients (including a carrier of a *GRN* mutation leading to TDP-43 pathology) and 2 nfPPA patients were included. We compared SUVr obtained at the usual early time window for [^{18}F]-AV-1451 PET acquisition (ET: 80–100 min) to a later acquisition window (LT: 190–210 min) between groups. Compared with ET, [^{18}F]-AV-1451 LT uptake in AD patients was significantly higher in the temporo-parietal cortex, and lower in subcortical regions. The LT window allowed to detect significantly increased tau binding in the frontal or temporal cortex in 3 bvFTD patients and in the 2 nfPPA patients that was not detectable with ET. The *GRN* mutation carrier showed no significant increase of tracer binding. [^{18}F]-AV-1451 late acquisition window could allow cortical binding to abnormal tau deposits to be revealed in a subset of bvFTD patients, which may distinguish them from the TDP-43 subtype.

Keywords Frontotemporal dementia · Neurofibrillary tangles · Tau pathology · Tau PET imaging · TDP-43

Abbreviations

AD	Alzheimer's disease
bvFTD	Behavioural frontotemporal dementia
nfPPA	Non-fluent/agrammatic variant of primary progressive aphasia
PET	Positron emission tomography
CDR	Clinical dementia rating
GCI	Global cortical index
MMSE	Mini-mental state examination
PiB	Pittsburgh compound B
SUVr	Standard uptake value ratio
ET	Early time window
LT	Late time window

Electronic supplementary material The online version of this article (https://doi.org/10.1007/s00415-019-09530-7) contains supplementary material, which is available to authorized users.

✉ Marie Sarazin
m.sarazin@ghu-paris.fr

[1] Unit of Neurology of Memory and Language, Université Paris Descartes, Sorbonne Paris Cité, Centre Hospitalier Sainte Anne, 1 rue Cabanis, 75014 Paris, France

[2] UMR 1023, IMIV, Service Hospitalier Frédéric Joliot, CEA, Inserm, Université Paris Sud, CNRS, Université Paris-Saclay, Orsay, France

[3] Department of Neurology, Centre Hospitalier Sainte-Anne, Inserm U894, Université Paris Descartes, Paris, France

[4] UNIACT, Neurospin, CEA, 91191 Gif-sur-Yvette, France

Introduction

In vivo assessment of regional tau protein load is now possible by means of positron emission tomography (PET) imaging [1]. Several tau tracers have been developed. Among them, [^{18}F]-AV-1451 (also called Flortaucipir) binds selectively to tau lesions composed primarily of paired helical filaments, such as intra and extra neuronal tangles and dystrophic neurites [2, 3]. In Alzheimer's disease (AD), the regional cortical distribution of [^{18}F]-AV-1451 binding is

congruent with the clinical presentation, and correlates with the Braak stages [4–6]. Sporadic AD patients also show unexpectedly high retention of the tracer in the basal ganglia, which is also present in healthy controls and considered to represent "off-target" tracer uptake [4, 6].

In non-AD tauopathies, however, the utility of tau PET imaging remains a matter of debate. While postmortem studies showed low or absent binding of [^{18}F]-AV-1451 to tau straight filaments [3, 7], recent publications reported tracer uptake in subcortical structures in corticobasal syndrome [8] and in the precentral gyrus, supplementary motor area and Broca's area in primary progressive apraxia of speech (PPAS) [9]. Increased tracer binding has also been reported in the temporal and frontal lobes as well as in the basal ganglia in *MAPT* mutation carriers presenting with behavioural frontotemporal degeneration (bvFTD), whose tau lesions are nevertheless quite similar to those found in AD [10, 11]. These observations prompt us to investigate more deeply the potential utility of [^{18}F]-AV-1451 PET in suspected non-AD tauopathies, especially sporadic bvFTD.

In pathological studies, tau lesions are found in about 40% of bvFTD cases, while TDP-43 lesions represent the majority of the remaining 60%, together with rare forms caused by FUS (Fused-in-Sarcoma) lesions. Two of the three studies using tau PET in sporadic bvFTD published to date are difficult to interpret because the patients studied were considered a homogeneous group, i.e., the neuropathological heterogeneity of the clinical entity was not taken into account, and reported increased tracer uptake restricted to subcortical regions, with no significant cortical binding [12, 13]. A third recent study nevertheless showed elevated frontal or temporal uptake in 2 out of 7 amyloid-negative sporadic bvFTD patients [14].

Based on the work of Barret et al. [15], which provided long kinetics extending up to 210 min, we performed kinetic analysis of [^{18}F]-AV-1451 time-activity curves and found that in AD, the ratio between high-binding structures and the cerebellum (used as reference region) is more stable at later acquisition times (LT: 190–210 min) than the earlier times (ET: 80–100 min) used so far in all published studies [16].

In the present work, we hypothesize that using later [^{18}F]-AV-1451 PET acquisition times, which could be better suited to the lower affinity of this tracer for the straight tau filaments present in non-AD tauopathies, would allow to detect tau pathology in a fraction of bvFTD patients and in patients with the non-fluent/agrammatic variant of primary progressive aphasia (nfPPA), which is most often underlain by tau pathology [17].

We first compared the [^{18}F]-AV-1451 uptake values measured in the early and late acquisition time windows in 16 early AD patients and 11 age-matched controls, aiming to confirm the earlier findings from Wimberley et al. To test our main hypothesis, we then assessed tracer uptake with these two time windows in seven bvFTD patients, one of whom carrying a *GRN* mutation guaranteeing TDP-43 underlying pathology, and in two nfPPA patients.

Material and methods

Study design and participants

We included 36 participants from the Shatau7-Imatau study (NTC02576821). The Ethics Committee (Comité de Protection des Personnes Ile-de-France VI) approved the study. All subjects provided written informed consent prior to participation.

Sixteen patients with typical (amnestic) AD were included according to current clinical and pathophysiological criteria, including positive CSF biomarkers and Pittsburgh compound B (PiB)-PET (Global cortical index − GCI > 1.45), as previously described [18], and a Clinical Dementia Rating (CDR) scale ≤ 1.

Seven patients with bvFTD were also included, using the criteria stipulated by the International bvFTD Criteria Consortium [19]. All had characteristic findings on neuroimaging (FDG-PET or SPECT), a cerebrospinal fluid (CSF) biomarkers profile not suggestive of AD, and negative amyloid imaging assessed by PiB-PET.

Two patients with nfPPA were included according to the consensus criteria [20]. Both had a CSF biomarkers profile not suggestive of AD, and negative PiB-PET.

Healthy elderly controls ($n = 11$) were recruited according to the following criteria: (i) Mini-Mental State Examination (MMSE) score ≥ 27/30 and normal neuropsychological assessment; (ii) CDR = 0; (iii) no history of neurological or psychiatric disorders; and (iv) negative PiB-PET.

Magnetic resonance imaging

Magnetic resonance imaging was performed at the Centre de Neuro-Imagerie de Recherche (CENIR, ICM, Paris) using a 3 T whole-body PRISMA 64-channel system (Siemens). The MRI examination included a three-dimensional (3D) T1-weighted volumetric magnetization-prepared rapid gradient echo (MP-RAGE) sequence (repetition time/echo time/flip angle: 2300 ms/3.43 ms/9°, inversion time = 900 ms, voxel size: $1 \times 1 \times 1$ mm^3), which provided a high grey/white matter contrast-to-noise ratio and enabled excellent segmentation and accurate coregistration with the PET images.

[^{11}C]-PiB and [^{18}F]-AV-1451 PET imaging procedure

Data acquisition

MRI and PET scans were performed within 4 months of each other. All PET examinations were acquired at Service Hospitalier Frédéric Joliot (Orsay, CEA). Amyloid-PET imaging was performed using [^{11}C]-PiB, followed on the same day by Tau-PET imaging using [^{18}F]-AV-1451. The latter was performed at least 3 h after administration of [^{11}C]-PiB to allow for complete decay of carbon-11 (half-life: 20.4 min). Both PET scans were performed on a High-Resolution Research Tomograph (HRRT; CTI/Siemens Molecular Imaging). A 6-min brain transmission scan using a ^{137}Cs point source was performed before each radiopharmaceutical administration to correct emission data for tissue attenuation. Amyloid-PET acquisition was performed from 40 to 60 min after injection of 332.2 ± 69 MBq of [^{11}C]-PiB. For Tau-PET, two acquisition windows were used: 80–100 min and 190–210 min after intravenous administration of 377.5 ± 34.4 MBq of [^{18}F]-AV-1451. Two bvFTD patients performed only one time window acquisition (patient #4 was unable to undergo the late scanning session; the early acquisition window was missed in patient #5 for technical reasons).

All post-processing image corrections (attenuation, normalization, random and scatter coincidences) were incorporated in an iterative ordinary Poisson ordered-subset expectation maximization (OP-OSEM) algorithm. Partial volume effect (PVE) was corrected by directly modeling the detector spatial resolution properties (i.e. Point Spread Function modeling) in the image reconstruction algorithm [21, 22], allowing improved spatial resolution of the image and thus reduced PVE, without applying a standard partial volume correction technique. Dynamic list mode acquisitions were binned into successive 5-min time frames. The noise equivalent count rates were calculated for each frame of each acquisition for each patient. The mean results for early and late time windows are 18,426 ± 3895 and 9801 ± 2136 respectively.

Volume of interest analysis

Parametric images were created using BrainVisa software (https://brainvisa.info) [23] by averaging the original 5-min images over 40–60 min after administration of [^{11}C]-PiB, and over 80–100 min and 190–210 min after administration of [^{18}F]-AV-1451. Standard Uptake Value ratio (SUVr) parametric images were obtained by dividing each voxel by the average value of the cerebellar grey matter region-of-interest eroded 4 mm in order to be at a distance from both the superior part of the vermis, which is a site of off target binding, and the adjacent structures (occipital cortex, CSF). This structure was used as reference region for analysis of both PET datasets as it is spared from amyloid plaques and tau accumulation in AD [3, 24, 25] and of tau lesions in FTLD-tau [26] and corticobasal denegeration [27] until the very late stages of the disease.

Automated segmentation of grey matter was performed on the 3D T1 MRI images of each subject using the SPM8 software (Institute of Neurology, London, UK; https://www.fil.ion.ucl.ac.uk/spm/). The Automated Anatomic Labeling (AAL) atlas was used to segment 76 cortical volumes of interest (VOI), which were warped in each subject's T1 space and were intersected with the subject's T1 MRI grey matter mask to perform pseudo atrophy correction. These VOIs based on individual MRI scans were then applied onto the subject's PET space for the three separate PET datasets (namely, [^{11}C]-PiB and the two [^{18}F]-AV1451 acquisition windows) following coregistration using standard mutual information algorithm. The VOIs, defined separately for the left and right hemispheres, were pooled into broader anatomical volumes of interest: we considered three left and right cortical volumes of interest: the frontal (with its inferolateral and superior sub-regions), parietal and temporal lobes. Subcortical nuclei (putamen, pallidum, thalamus) were segmented with the volBrain® online web interface (https://volbrain.upv.es) [28]. To quantify tau tracer uptake in the frontal white matter, we eroded the white matter mask (2 mm from the white matter surface) and intersected it with a manually-drawn VOI corresponding to an expansion of frontal cortical parcellation. We chose a 2 mm erosion as it is close to the intrinsic resolution of the HRRT PET camera. This choice was a compromise between being far enough from adjacent structures without reducing too much the volume of the final VOI. We verified that modifying the degree of erosion of the frontal white matter (up to 3 or 4 mm) did not affect our results.

We averaged the left and right SUVr values in each region studied in order to obtain a unique value per cortical (frontal, parietal and temporal lobes) or subcortical (putamen, pallidum, thalamus, frontal white matter) region.

Statistical analysis

Data were analysed using STATISTICA 6 software (Statsoft). Differences between groups were assessed using a Mann–Whitney test, and comparisons of the SUVRs between early and late time windows within each group were assessed using non-parametric tests for paired samples (Sign test). A Bonferroni correction was used for multiple comparisons. As the bvFTD group was heterogeneous regarding tau PET binding, subjects were analyzed individually vs the control group using *Z*-scores, which are standard deviations (σ). $1.96 \times \sigma$ corresponds to a 95% confidence interval. *Z*-scores higher than 1.96 were considered significant.

Results

The main demographic, clinical, amyloid imaging and biological data for the control, AD and bvFTD groups, and separately for each bvFTD and nfPPA patient, are summarized in Table 1. There was no significant difference in age, sex ratio and educational level between groups.

Early (ET) versus late time (LT) window regional [^{18}F]-AV-1451 SUVr in controls and AD patients

On visual inspection, all controls had low tracer binding (Fig. 1a). The SUVr remained stable ($p > 0.05$) between ET and LT in cortical lobes apart from a small increase with LT for the parietal lobe ($p < 0.05$), but decreased significantly in all subcortical nuclei (all $p < 0.003$) (Table 2, Fig. 2).

On visual inspection, all AD patients had high tracer binding, especially in the temporo-parietal cortices (Fig. 1b). Relative to controls, the SUVr values were significantly increased in the AD group in all cortical regions for both ET and LT (all $p < 0.003$), the highest values being observed for the temporal and parietal cortices. In the AD group, the SUVr values increased between ET and LT in all cortical regions, significantly so for the temporal and parietal cortices ($p < 0.003$), while LT values were significantly lower for all the subcortical nuclei (all $p < 0.003$) (Table 2, Fig. 2). Individual comparisons of AD patients with the control group using *Z*-scores are detailed in supplementary Table 1.

Regional [^{18}F]-AV-1451 SUVr values in bvFTD and nfPPA patients

On visual inspection, [^{18}F]-AV-1451 uptake varied greatly from patient to patient, especially at LT in the bvFTD group (Fig. 1). As a group, no significant regional differences from controls were found for either the ET and LT acquisition windows. Considering the known heterogeneity of bvFTD neuropathology, as well as the heterogeneity of visual analyses of tau-PET imaging, we analysed individual SUVr values for each patient expressed as *Z*-scores (compared with the control group) in each VOI. Individually, no regional cortical tau SUVr value obtained with the ET window was outside the normal range in any bvFTD patient. In contrast, the *Z*-scores for the LT acquisition window were positive (> 1.96) for the frontal lobe, frontal sub-regions, or temporal lobe in 3 bvFTD patients. Regarding the deep nuclei, the *Z*-scores were positive (> 1.96) for the putamen in three patients and the pallidum in two, with higher mean SUVr values at LT than at ET (even if the difference was not statistically significant). Finally, the *Z*-scores for the frontal white matter became positive with LT in the latter 3 patients (Table 2).

The patient who carried a *GRN* mutation showed no significant increase of tau tracer uptake for any VOI with either time window (Table 2, Fig. 1c).

One nfPPA patient had a slightly increased tracer uptake in a subregion of the frontal cortex at ET. Using LT acquisition, both nfPPA patients were clearly positive in the frontal cortex, as well as in the parietal cortex and subcortical structures for patient #2 (Table 2, Fig. 3).

Discussion

Based on a previous report in AD [16], in the present study we assessed whether - as opposed to the usually recommended and standard earlier acquisition window - late acquisition [^{18}F]-AV-1451 PET combined with individual subject PET data analysis would be more sensitive to detect cortical tau deposits in at least a fraction of bvFTD patients. First, our data in AD confirmed that late acquisition led to an increase in [^{18}F]-AV-1451 cortical uptake, especially in the temporo-parietal cortex, together with a decrease in tracer uptake in all subcortical regions, the latter being also observed in healthy subjects. Second, in bvFTD the late acquisition window allowed to detect significant tau tracer binding in 3 patients in the frontal or temporal cortex that was missed by the early acquisition window. The same result was obtained in both nfPPA patients included. Furthermore, as expected given the TDP-43 underlying pathology, the carrier of a *GRN* mutation showed no significant increase of tracer binding even using late acquisition data.

One difficulty observed in the numerous publications with [^{18}F]-AV-1451 PET is the presence of high tracer uptake in subcortical regions (putamen, pallidum, and to a lesser degree thalamus) in both controls and AD patients. The cause of this 'off-target' non-specific uptake, which is independent of amyloid burden, is not totally understood [3, 29]. A recent study in AD patients and controls showed an association between the tracer uptake in the basal ganglia and the age-related iron accumulation [30]. Off-target binding of tau tracer to MAO-B has also been reported, which could complicate the use of the cerebellum as a reference region [31]. Nevertheless, this off-target binding to MAO is still debated for [^{18}F]-AV-1451, especially in humans [32].

Our data confirm that using a later time window for [^{18}F]-AV-1451 PET image acquisition leads to increases in tracer binding in affected cortical areas, while at the same time attenuates the off-target uptake in subcortical regions in AD as well as in controls. In favour of this observation, the decrease of the SUVr in the basal ganglia was of the same order of magnitude in AD patients and in controls. On the contrary, the tracer binding increases in the affected cortical areas were clearly more pronounced in AD patients, in agreement with the idea that the LT window could enhance

Table 1 Characteristics of the subjects

	Controls mean (SD)	AD patients mean (SD)	bvFTD patients ($n=7$)							nfPPA patients ($n=2$)	
	$n=11$	$n=16$	#1	#2	#3	#4	#5	#6	#7	#1	#2
Age	68.9 (3.3)	67.7 (7.1)	62	66	73	74	70	69	76	63	69
Sex	7F/4M	8F/8M	M	M	M	F	F	F	M	F	F
Education (yrs)	15.2 (3.1)	14.2 (4)	6	11	18	9	9	15	19	17	17
Disease duration (yrs)	NA	5.4 (4.3)	3	2	4	6	2	2	6	5	4
MMSE	28.6 (1)	23.9 (3)*	13	23	25	16	10	18	25	28	24
Neurological examination	Normal	Normal	Normal, no MND	Normal, no MND	Normal, no MND	Normal, no MND	Normal, no MND	Normal, no MND	Normal, no MND	No parkinsonism Speech apraxia	Parkinsonism Speech apraxia then anarthria
CSF[a]											
Tau	NA	573 (176)	443	163	267	433	179	225	555	508	554
pTau	NA	88 (40)	46	29	38	52	32	26	77	68	78
Aß	NA	461 (154)	976	615	657	1196	691	590	1466	1251	620
PiB GCI	1.27 (0.1)	2.98 (0.64)*	1.18	1.13	1.42	1.11	Negative[b]	1.18	1.3	1.25	1.4
Pl. PGRN (µg/l)	132.2 (25.8)	114.2 (32.8)	52	107	89	106	80	132	191	134	130
ApoE	E3/E3 $n=9$	E3/E3 $n=4$	E3/E3	E3/E3	E3/E3	E3/E3	E3/E3	E3/E3	E2/E3	E3/E3	E3/E4
		E4/E4 $n=2$									
	E2/E3 $n=1$	E2/E3 $n=1$									
	E3/E4 $n=1$	E3/E4 $n=9$									
FTD mutations (*c9orf72* or *GRN*)	NA	NA	c.709-1G > A mutation (intron 7) of the *GRN* gene	None	None	None	None	None	None	None	None

Main demographic, clinical, amyloid imaging and biological data for the control and AD groups, and for each bvFTD and nfPPA patient

bvFTD behavioural-variant frontotemporal dementia, *AD* Alzheimer's disease, *nfPPA* non-fluent/agrammatic primary progressive aphasia, *SD* standard deviation, *MMSE* mini-mental state examination, *MND* motor neuron disease, *CSF* cerebrospinal fluid, *pTau* phosphorylated tau protein, *Aß* amyloid peptide, *PiB-GCI* Pittsburgh compound B global cortical index, *Pl PGRN* plasmatic progranulin, *ApoE* Apolipoprotein E

*$p<0.001$ relative to controls

[a]Values shown are in pg/ml

[b]PiB GCI not measurable for technical reasons, but clearly negative on visual inspection

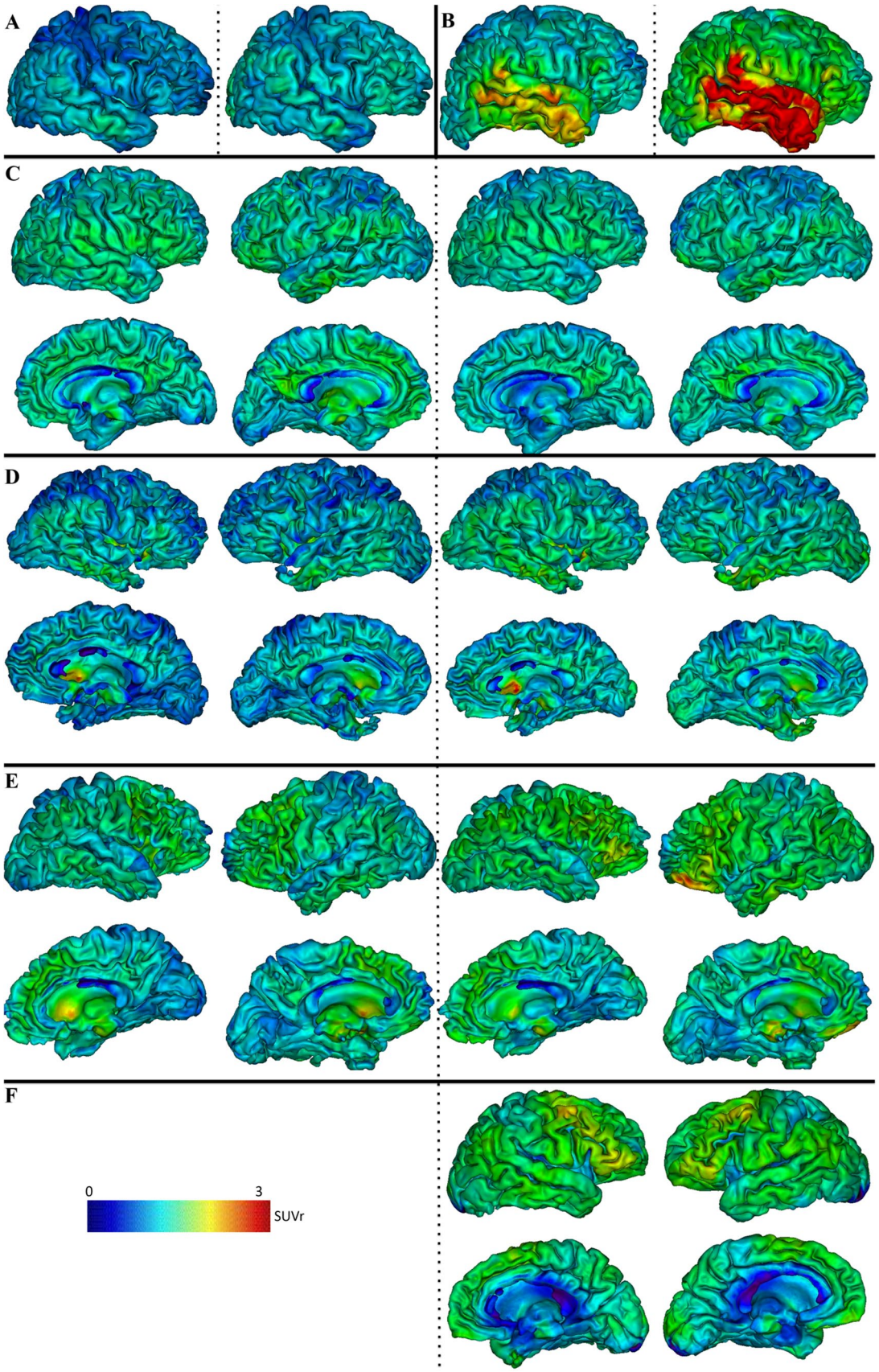
A
B
C
D
E
F
0
3
SUVr

◂**Fig. 1** Cortical [^{18}F]-AV-1451 SUVr in one control subject, one AD patient and four bvFTD patients. Projection of the cortical [^{18}F]-AV-1451 SUVr on the individual 3D mesh MRI at early (left side of each panel) and late (right side of each panel) acquisition time windows (separated by the dotted line) in one control subject (**a**), one AD patient (**b**), bvFTD patient #1 (*GRN* mutation carrier) (**c**), bvFTD patient #7 (**d**), bvFTD patient #6 (**e**) and bvFTD patient #5 (**f**). Lateral views of the right hemisphere are shown for the control and AD patient. Lateral (top row) and medial (bottom row) views of each hemisphere are shown for the bvFTD patients

the capacity of [^{18}F]-AV-1451 to identify tau binding. Even if the SUVr at this late acquisition time may somewhat overestimate the total volume of distribution (V_T) as measured by compartmental analysis [15], our results suggest that it could be a sensitive index of tracer binding on tau deposits by increasing the contrast between tau-rich regions and non specific or off target binding regions. Baker et al. (2017) showed that later time periods than the 80–100 min interval provided better agreement between reference standards and SUVRs for ROIs with high tracer binding [33]. Studies using compartmental analysis showed that SUVr at the time periods of 80–100 or 130 min were better correlated to the V_T [15, 34]. Unfortunately, to our knowledge, no direct comparison was made between the V_T at 210 min and SUVr at 210 min.

Beyond applications in AD, this methodological point appears of considerable interest when investigating non-AD tauopathies using [^{18}F]-AV-1451, because the affinity of this tau tracer for non-AD tau lesions may be lower than that for AD tauopathy [3, 7]. Using ET, not only the quantification of [^{18}F]-AV-1451 uptake in subcortical structures, including the white matter, could be contaminated by non–tau-related signal, but also detection of cortical tau pathology may be altogether missed [35].

Using the LT acquisition window, significant frontal or temporal lobe tau tracer binding was detected in 3/6 patients (one patient had no LT acquisition), which went undetected in two of them using the ET window. The regional distribution of cortical tau binding was consistent with that of expected pathological lesions in bvFTD. In spite of the small size of our bvFTD group, this proportion is close to that expected on the basis of neuropathological data, namely ~ 40% of tau pathology in bvFTD. This finding likely reflects tau pathology, as both nfPPA patients also showed increased tracer binding at LT in frontal and parietal regions, which was not found, or at least much less pronounced at ET. Of note, both nfPPA patients had speech apraxia, which has been reported to be a predictor of tau pathology [36]. In order to avoid atypical AD, we used strict inclusion criteria, including negative PiB-PET.

The increased tracer binding in bvFTD and nfPPA patients, especially bvFTD patient #6 and nfPPA patient #2 cannot be attributed to a non-specific effect of disease severity, as these patients were not the most clinically impaired according to the MMSE score and functional scales. The influence of amyloid burden on tau tracer binding in these non-AD patients is also unlikely as the patients with higher tau tracer retention are not those who have the higher PiB-GCI or the lower CSF Aß level.

Only three published articles so far have reported [^{18}F]-AV-1451 PET imaging in sporadic bvFTD, all using the standard ET acquisition window, two of which showing increased subcortical uptake only, affecting the white matter and basal ganglia [12, 13]. In these two articles, the PET data were presented for the entire group only, i.e., individual subject analysis was not reported. Our results are in accordance with those of the third study published recently [14], even if we obtained binding positivity at LT and not at ET. In other suspected non-AD tauopathies such as the corticobasal syndrome, increased tau tracer uptake, again derived using the ET window, was found in the globus pallidus, subthalamic nucleus, midbrain and dentate nucleus of the cerebellum [8], but the authors' interpretation was uncertain given the possibility of off-target binding in subcortical regions.

To our knowledge, tau PET imaging has not been reported so far in amyloid-negative *GRN* mutation carriers, as the patient described recently in another study had positive PiB-PET [14]. Our finding of normal tracer uptake in all cortical and subcortical VOIs assessed is of interest as it confirms the absence of tau tracer binding in established TDP-43 pathology. Surprisingly, recent studies in semantic dementia, which is mainly—though not always—associated with TDP-43 pathology, found increased tau tracer uptake in anterior temporal areas [37, 38]. This unexpected observation could be explained by some biological or chemical differences in the TDP-43 pathology associated with *GRN* mutation versus sporadic semantic dementia, as the former is related to TDP-43 type A [39] and the latter to TDP-43 type C lesions [17].

Our study has some limitations, especially the small bvFTD sample size and the lack of neuropathological confirmation. So the results should be interpreted with caution. However, the patients reported in our study were included based on strict criteria (see Methods), and within-subject data analysis was carried out. Furthermore, the behavioral disturbances that affect bvFTD patients can make it difficult to obtain exploitable PET results, thus inevitably leading to small samples and missing data. The bvFTD patients were not screened for *MAPT* mutations, which are only looked for in patients younger than 65 years in clinical practice. All our patients, except the *GRN* mutation carrier and an nfPPA patient, were older than 65 at disease onset. In view of these considerations and given the rarity of *MAPT* mutations, the probability that the tau tracer binding found here only reflects the already studied tauopathy associated with *MAPT* mutations is very low. Another limitation relates to the late

Table 2 Detailed tau PET data

	Groups: mean SUVr (SD)						bvFTD patients: mean SUVr (individual *Z*-scores)					
	Controls $n=11$		AD $n=16$		bvFTD $n=7$		#1 (*GRN* mutation)		#2		#3	
	ET	LT	ET	LT	ET	LT	ET	LT	ET	LT	ET	LT
Frontal	1.23 (0.13)	1.32 (0.15)	1.75 (0.57)*	1.95 (0.8)*	1.24 (0.09)	1.31 (0.22)	1.31 (0.61)	1.22 (− 0.7)	1.17 (− 0.5)	1.17 (− 1)	1.19 (− 0.3)	1.07 (− 1.7)
Lat OF	1.31 (0.15)	1.53 (0.18)§	–	–	1.34 (0.13)	1.53 (0.29)	1.47 (1.06)	1.37 (− 0.9)	1.18 (− 0.9)	1.23 (− 1.7)	1.32 (0.07)	1.34 (− 1.1)
IF PT	1.28 (0.16)	1.4 (0.2)§	–	–	1.34 (0.12)	1.44 (0.29)	1.41 (0.8)	1.37 (− 0.1)	1.28 (0)	1.22 (− 0.9)	1.21 (− 0.4)	1.15 (− 1.3)
Frontal sup	1.19 (0.13)	1.26 (0.14)	–	–	1.17 (0.1)	1.23 (0.27)	1.2 (0.1)	1.06 (− 1.4)	1.14 (− 0.4)	1.16 (− 0.7)	1.11 (− 0.6)	0.91 (− 2.5)
Temporal	1.22 (0.13)	1.22 (0.16)	2.2 (0.9)*	2.65 (1.2)*§	1.21 (0.09)	1.22 (0.18)	1.27 (0.4)	1.24 (0.1)	1.16 (− 0.5)	1.12 (− 0.6)	1.04 (− 1.4)	0.93 (− 1.8)
Inf. Temp	1.28 (0.14)	1.26 (0.14)	2.6 (1.1)*	3.03 (1.27)* §	1.35 (0.13)	1.35 (0.22)	1.33 (0.4)	1.37 (0.8)	1.25 (− 0.2)	1.24 (− 0.1)	1.18 (− 0.7)	1.03 (− 1.6)
Parietal	1.18 (0.14)	1.29 (0.18)§	2 (0.75)*	2.45 (1.1)*§	1.17 (0.08)	1.28 (0.18)	1.24 (0.43)	1.26 (− 0.2)	1.26 (0.6)	1.3 (0.05)	1.02 (− 1.1)	0.95 (− 1.9)
Putamen	1.61 (0.19)	1.3 (0.17)§	1.82 (0.3)	1.51 (0.19)§	1.94 (0.4)	1.5 (0.58)	1.53 (− 0.4)	1.34 (0.2)	1.56 (− 0.3)	1.11 (− 1.1)	1.69 (0.4)	1.03 (− 1.6)
Thalamus	1.29 (0.15)	1.03 (0.15)§	1.39 (0.2)	1.14 (0.18)§	1.41 (0.15)	1.1 (0.23)	1.54 (1.7)	1.29 (1.7)	1.44 (1)	0.91 (− 0.8)	1.15 (− 0.9)	0.8 (− 1.5)
Pallidum	1.92 (0.3)	1.52 (0.26)§	2.03 (0.35)	1.6 (0.22)§	2.13 (0.37)	1.81 (0.7)	1.91 (− 0.03)	1.52 (0)	1.95 (0.1)	1.28 (− 0.9)	1.72 (− 0.7)	1.09 (− 1.7)
Frontal white matter	1.36 (0.19)	1.24 (0.19)	1.64 (0.3)	1.56 (0.3)*	1.57 (0.11)	1.46 (0.23)	1.6 (1.26)	1.41 (0.9)	1.48 (0.6)	1.38 (0.7)	1.43 (0.4)	1.06 (− 0.9)

	bvFTD patients: mean SUVr (individual *Z*-scores)								nfPPA patients: mean SUVr (individual *Z*-scores)			
	#4		#5		#6		#7		#1		#2	
	ET	LT	ET	LT	ET	LT	ET	LT	ET	LT	ET	LT
Frontal	1.3 (0.5)	NA	NA	**1.62 (2)**	1.36 (1)	1.55 (1.5)	1.13 (− 0.8)	1.26 (− 0.4)	1.3 (0.5)	1.57 (1.7)	1.24 (0.1)	**1.65 (2.2)**
Lat OF	1.38 (0.5)	NA	NA	1.83 (1.7)	1.48 (1.1)	**1.96 (2.4)**	1.2 (− 0.7)	1.46 (− 0.4)	**1.67 (2.4)**	**2.47 (5.2)**	1.28 (− 0.2)	1.78 (1.4)
IF PT	1.47 (1.2)	NA	NA	**1.81 (2)**	1.46 (1.1)	**1.81 (2)**	1.23 (− 0.3)	1.31 (− 0.4)	1.42 (0.9)	1.69 (1.5)	1.27 (− 0.1)	1.76 (1.8)
Frontal sup	1.18 (− 0.1)	NA	NA	**1.66 (2.9)**	1.34 (1.2)	1.43 (1.2)	1.04 (− 1.2)	1.15 (− 0.8)	1.17 (− 0.2)	1.21 (− 0.4)	1.26 (0.5)	**1.67 (2.9)**
Temporal	1.25 (0.2)	NA	NA	1.29 (0.4)	1.25 (0.2)	1.32 (0.6)	1.29 (0.5)	1.44 (1.4)	1.26 (0.3)	1.31 (0.6)	1.19 (− 0.2)	1.43 (1.3)
Inf. Temp	1.39 (0.8)	NA	NA	1.32 (0.4)	1.41 (0.9)	1.43 (1.2)	1.55 (1.9)	**1.68 (3)**	1.2 (− 0.5)	1.27 (0.1)	1.25 (− 0.2)	1.45 (1.4)
Parietal	1.1 (− 0.2)	NA	NA	1.43 (0.8)	1.21 (0.2)	1.44 (0.8)	1.15 (− 0.2)	1.27 (− 0.1)	1.21 (0.2)	1.38 (0.5)	1.19 (0.1)	**1.64 (1.96)**
Putamen	**2.2 (3.1)**	NA	NA	1.26 (− 0.2)	**2.05 (2.3)**	**1.66 (2.1)**	**2.57 (5)**	**2.59 (7.6)**	1.38 (− 1.2)	0.95 (− 2)	1.67 (0.3)	**1.7 (2.3)**
Thalamus	1.37 (0.5)	NA	NA	0.98 (− 0.3)	1.56 (1.8)	1.25 (1.5)	1.4 (0.7)	**1.36 (2.2)**	1.04 (− 1.7)	0.85 (− 1.2)	1.39 (0.7)	**1.51 (3.2)**
Pallidum	2.06 (0.5)	NA	NA	1.68 (0.6)	**2.5 (1.9)**	**2.4 (3.4)**	**2.66 (2.5)**	**2.9 (5.3)**	1.46 (− 1.5)	1 (− 2)	1.9 (− 0.1)	**2.06 (2.1)**
Frontal white matter	1.69 (1.7)	NA	NA	1.53 (1.5)	1.71 (1.8)	**1.72 (2.5)**	1.5 (0.7)	**1.64 (2.1)**	1.11 (− 1.3)	0.95 (− 1.5)	1.46 (0.5)	**1.92 (3.6)**

Tau PET SUVr (standardized uptake value ratio): mean (standard deviation) in control, AD and bvFTD groups, and mean SUVr (individual *Z*-scores) in bvFTD and nfPPA patients. Significant differences with controls (95% confidence level) are indicated by bold

AD Alzheimer's disease, *bvFTD* behavioural variant of frontotemporal dementia, *nfPPA* non-fluent/agrammatic primary progressive aphasia, *ET* early time window, *LT* late time window, *Lat OF* lateral orbitofrontal cortex, *IF PT* inferior frontal cortex pars triangularis, *Frontal sup* superior frontal cortex, *Inf. Temp.* inferior temporal cortex, *NA* missing data

*$p<0.003$ vs controls (Bonferroni correction for fourteen tests)

§$p<0.005$ in the comparison between ET and LT (Bonferroni correction for nine tests)

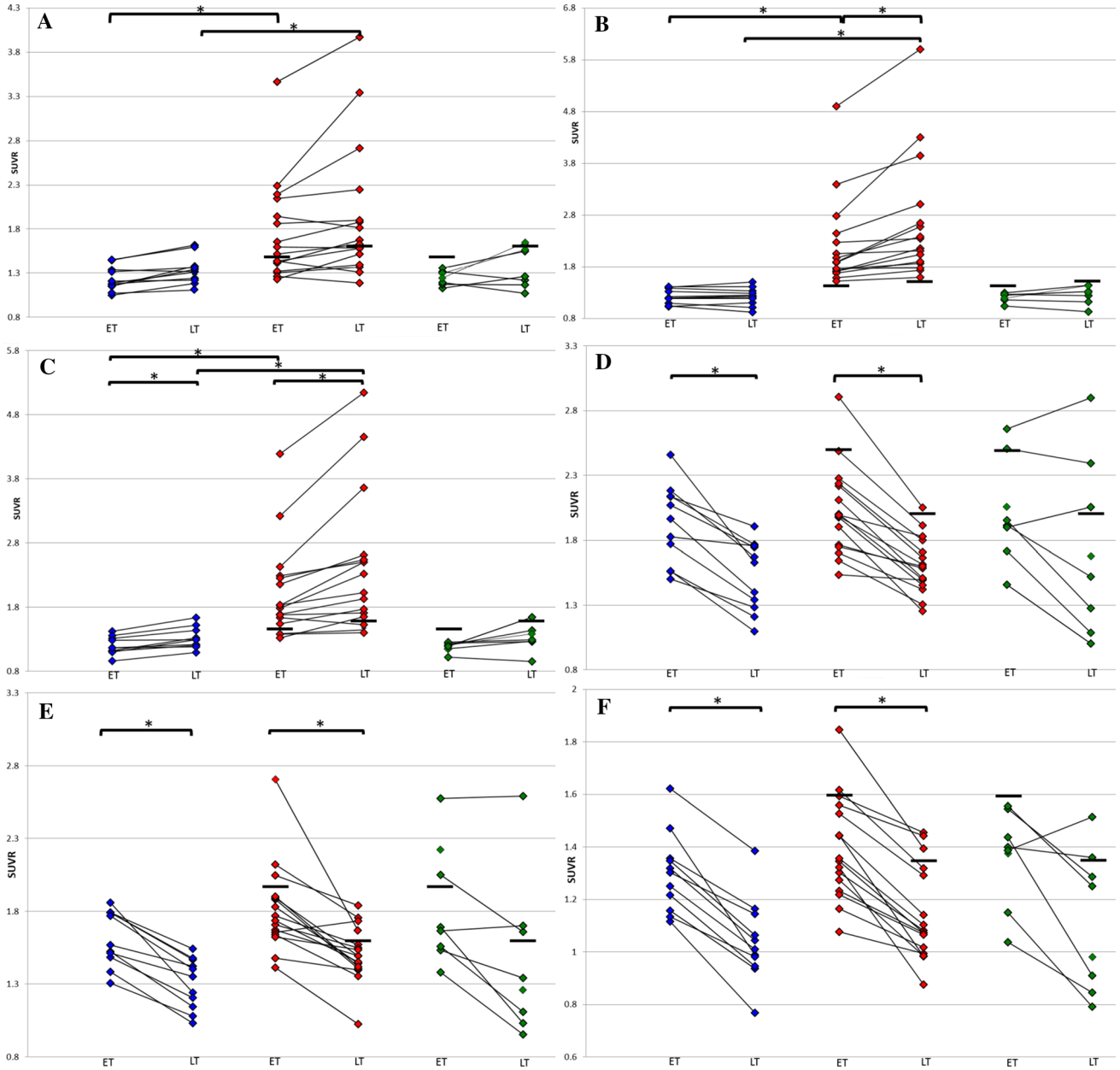

Fig. 2 SUVr in healthy controls, AD patients and bvFTD/nfPPA patients at the early and late acquisition time windows. Scatter plot showing [^{18}F]-AV-1451 standard uptake value ratios (SUVr) obtained in healthy controls (blue diamonds), AD patients (red diamonds) and bvFTD/nfPPA patients (green diamonds), at both the early and late acquisition time windows (ET and LT, respectively) for the frontal (**a**), temporal (**b**) and parietal (**c**), as well as for the pallidum (**d**), putamen (**e**) and thalamus (**f**) volumes of interest. Horizontal black lines represent the 95% upper confidence limit (i.e., *Z*-score = 1.96) derived from healthy controls (see Methods). *$p < 0.003$ for the comparisons between AD patients and controls, and between SUVr values obtained with the early and late acquisition time windows in each patient group. *AD* Alzheimer's disease, *SUVr* standardized uptake value ratio

acquisition time window images, which may be affected by the inevitably higher noise resulting from radioactive decay [16]. However this limitation can be compensated for by longer time frame acquisitions, and other time windows situated between the two considered here could be tested.

Conclusion

Despite these caveats, our results suggest that the [^{18}F]-AV-1451 late acquisition window is of potential interest to identify the tauopathy present in a subset of bvFTD patients, and in turn to distinguish this subgroup from TDP-43-related bvFTD. Another distinct advantage of the late

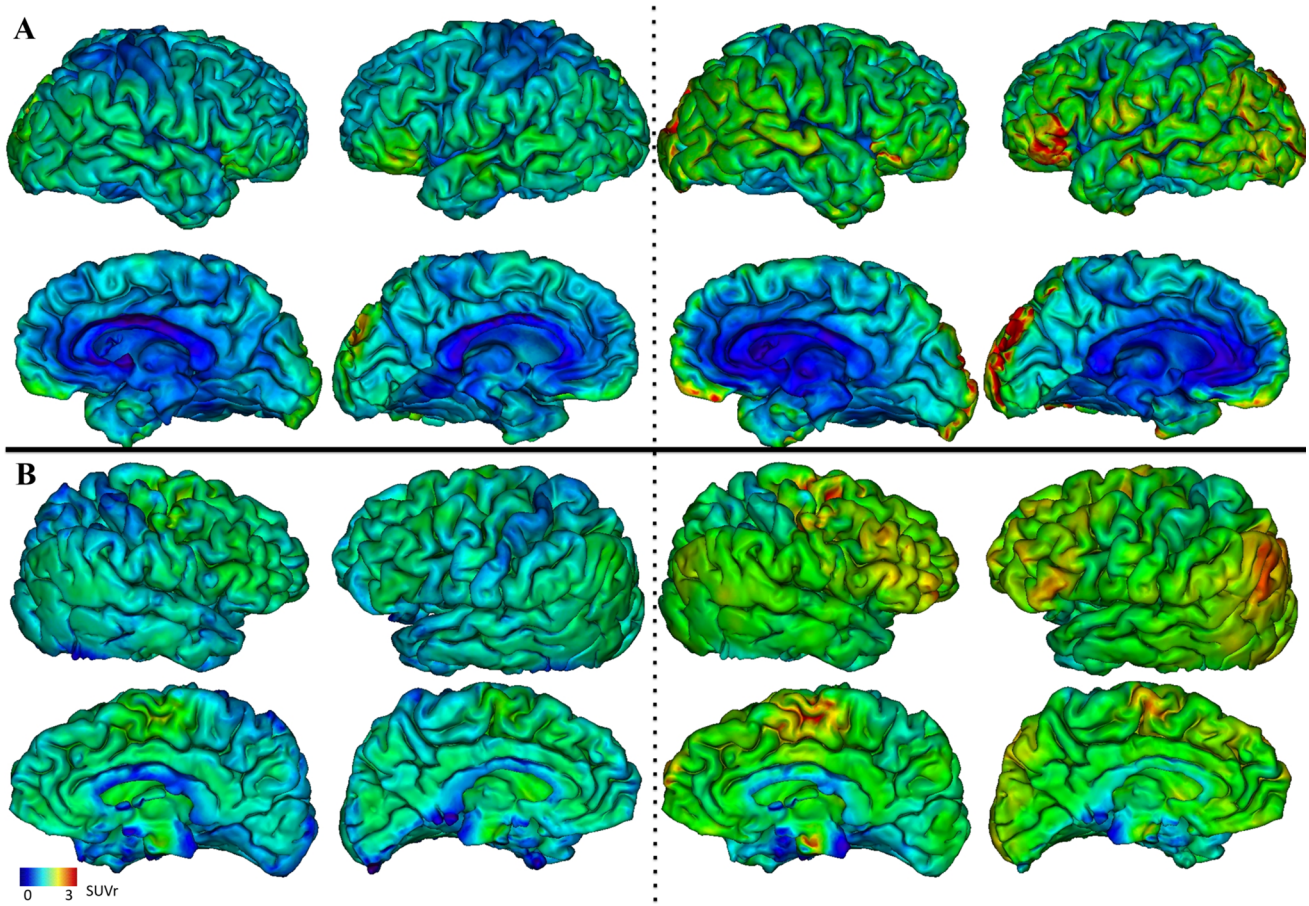

Fig. 3 Cortical [^{18}F]-AV-1451 SUVr in the two nfPPA patients. Projection of the cortical [^{18}F]-AV-1451 SUVr on the individual 3D mesh MRI at early (left side of each panel) and late (right side of each panel) acquisition time windows (separated by the dotted line) in nfPPA patient #1 (**a**) and nfPPA patient #2 (**b**). Lateral (top row) and medial (bottom row) views of each hemisphere are shown

acquisition images is the marked decrease in subcortical 'off-target' binding. These promising observations will need to be confirmed in a larger cohort.

Acknowledgements The authors are grateful to the chemical/radiopharmaceutical and nursing staff of the Service Hospitalier Frederic Joliot for the synthesis of [^{11}C]-PIB and [^{18}F]-AV-1451 and patient management, respectively, the staff of the Centre de Neuroimagerie de Recherche (CENIR), Salpêtrière Hospital, for patient management during MRI acquisition.

We are also indebted to AVID Radiopharmaceuticals, Inc., for their support in supplying the AV- 1451 precursor and chemistry production advice.

Funding This study was funded by the French Ministry of Health grant (PHRC-2013-0919), CEA, Fondation pour la recherche sur Alzheimer, Institut de recherche internationale Servier, France-Alzheimer.

Compliance with ethical approval

Conflicts of interest The authors declare that they have no conflict of interest.

Ethical approval All procedures performed in studies involving human participants were in accordance with the ethical standards of the institutional and/or national research committee and with the 1964 Helsinki declaration and its later amendments or comparable ethical standards.

Informed consent Informed consent was obtained from all individual participants included in the study.

References

1. Villemagne VL, Fodero-Tavoletti MT, Masters CL et al (2015) Tau imaging: early progress and future directions. Lancet Neurol 14:114–124
2. Chien DT, Bahri S, Szardenings AK et al (2013) Early clinical PET imaging results with the novel PHF-tau radioligand [F-18]-T807. J Alzheimers Dis 34:457–468
3. Marquié M, Normandin MD, Vanderburg CR et al (2015) Validating novel tau positron emission tomography tracer [F-18]-AV-1451 (T807) on postmortem brain tissue. Ann Neurol 78:787–800

4. Schöll M, Lockhart SN, Schonhaut DR et al (2016) PET imaging of tau deposition in the aging human brain. Neuron 89:971–982
5. Schwarz AJ, Yu P, Miller BB et al (2016) Regional profiles of the candidate tau PET ligand 18F-AV-1451 recapitulate key features of Braak histopathological stages. Brain 139:1539–1550
6. Marquié M, Siao Tick Chong M, Antón-Fernández A et al (2017) [F-18]-AV-1451 binding correlates with postmortem neurofibrillary tangle Braak staging. Acta Neuropathol 134:619–628
7. Lowe VJ, Curran G, Fang P et al (2016) An autoradiographic evaluation of AV-1451 Tau PET in dementia. Acta Neuropathol Commun 4:58
8. Cho H, Baek MS, Choi JY et al (2017) 18F-AV-1451 binds to motor-related subcortical gray and white matter in corticobasal syndrome. Neurology 89:1170–1178
9. Utianski RL, Whitwell JL, Schwarz CG et al (2018) Tau-PET imaging with [18F]AV-1451 in primary progressive apraxia of speech. Cortex 99:358–374
10. Smith R, Puschmann A, Schöll M et al (2016) 18F-AV-1451 tau PET imaging correlates strongly with tau neuropathology in MAPT mutation carriers. Brain 139:2372–2379
11. Spina S, Schonhaut DR, Boeve BF et al (2017) Frontotemporal dementia with the V337M MAPT mutation: Tau-PET and pathology correlations. Neurology 88:758–766
12. Cho H, Seo SW, Choi JY et al (2018) Predominant subcortical accumulation of 18F-flortaucipir binding in behavioral variant frontotemporal dementia. Neurobiol Aging 66:112–121
13. Son HJ, Oh JS, Roh JH et al (2019) Differences in gray and white matter 18F-THK5351 uptake between behavioral-variant frontotemporal dementia and other dementias. Eur J Nucl Med Mol Imaging 46:357–366
14. Tsai RM, Bejanin A, Lesman-Segev O et al (2019) 18F-flortaucipir (AV-1451) tau PET in frontotemporal dementia syndromes. Alzheimers Res Ther 11:13
15. Barret O, Alagille D, Sanabria S et al (2017) Kinetic Modeling of the Tau PET Tracer 18F-AV-1451 in Human Healthy Volunteers and Alzheimer Disease Subjects. J Nucl Med 58:1124–1131
16. Wimberley C, Lagarde J, Olivieri P et al (2018) Optimal time window for [^{18}F]-AV-1451 binding quantification in AD using SUVr [abstract]. In: 12th Human Amyloid Imaging, Miami January 17–19 2018, p101.
17. Spinelli EG, Mandelli ML, Miller ZA et al (2017) Typical and atypical pathology in primary progressive aphasia variants. Ann Neurol 81:430–443
18. Hamelin L, Lagarde J, Dorothée G et al (2016) Early and protective microglial activation in Alzheimer's disease: a prospective study using 18F-DPA-714 PET imaging. Brain 139:1252–1264
19. Rascovsky K, Hodges JR, Knopman D et al (2011) Sensitivity of revised diagnostic criteria for the behavioural variant of frontotemporal dementia. Brain 134:2456–2477
20. Gorno-Tempini ML, Hillis AE, Weintraub S et al (2011) Classification of primary progressive aphasia and its variants. Neurology 76:1006–1014
21. Sureau FC, Reader AJ, Comtat C et al (2008) Impact of image-space resolution modeling for studies with the high-resolution research tomograph. J Nucl Med 49:1000–1008
22. Varrone A, Sjöholm N, Eriksson L et al (2009) Advancement in PET quantification using 3D-OP-OSEM point spread function reconstruction with the HRRT. Eur J Nucl Med Mol Imaging 36:1639–1650
23. Mangin JF, Rivière D, Cachia A et al (2004) A framework to study the cortical folding patterns. Neuroimage 23(Suppl 1):S129–S138
24. Joachim CL, Morris JH, Selkoe DJ (1989) Diffuse senile plaques occur commonly in the cerebellum in Alzheimer's disease. Am J Pathol 135:309–319
25. de Souza LC, Corlier F, Habert M-O et al (2011) Similar amyloid-β burden in posterior cortical atrophy and Alzheimer's disease. Brain 134:2036–2043
26. Irwin DJ, Brettschneider J, McMillan CT et al (2016) Deep clinical and neuropathological phenotyping of Pick disease. Ann Neurol 79:272–287
27. Forman MS, Zhukareva V, Bergeron C et al (2002) Signature tau neuropathology in gray and white matter of corticobasal degeneration. Am J Pathol 160:2045–2053
28. Manjón JV, Coupé P (2016) volBrain: an online MRI brain volumetry system. Front Neuroinform 10:30
29. Marquié M, Verwer EE, Meltzer AC et al (2017) Lessons learned about [F-18]-AV-1451 off-target binding from an autopsy-confirmed Parkinson's case. Acta Neuropathol Commun 5:75
30. Choi JY, Cho H, Ahn SJ et al (2018) Off-target 18F-AV-1451 binding in the basal ganglia correlates with age-related iron accumulation. J Nucl Med 59:117–120
31. Drake LR, Pham JM, Desmond TJ et al (2019) Identification of AV-1451 as a weak, nonselective inhibitor of monoamine oxidase. ACS Chem Neurosci 10:3839–3846
32. Hansen AK, Brooks DJ, Borghammer P (2018) MAO-B inhibitors do not block in vivo flortaucipir ([$_{18}$F]-AV-1451) binding. Mol Imaging Biol 20:356–360
33. Baker SL, Lockhart SN, Price JC et al (2017) Reference tissue-based kinetic evaluation of 18F-AV-1451 for tau imaging. J Nucl Med 58:332–338
34. Wooten DW, Guehl NJ, Verwer EE et al (2017) Pharmacokinetic evaluation of the tau PET radiotracer 18F–T807 (18F-AV-1451) in human subjects. J Nucl Med 58:484–491
35. Schonhaut DR, McMillan CT, Spina S et al (2017) 18 F-flortaucipir tau positron emission tomography distinguishes established progressive supranuclear palsy from controls and Parkinson disease: a multicenter study. Ann Neurol 82:622–634
36. Harris JM, Gall C, Thompson JC et al (2013) Classification and pathology of primary progressive aphasia. Neurology 81:1832–1839
37. Bevan-Jones WR, Cope TE, Jones PS et al (2018) [18F]AV-1451 binding in vivo mirrors the expected distribution of TDP-43 pathology in the semantic variant of primary progressive aphasia. J Neurol Neurosurg Psychiatry 89:1032–1037
38. Makaretz SJ, Quimby M, Collins J et al (2018) Flortaucipir tau PET imaging in semantic variant primary progressive aphasia. J Neurol Neurosurg Psychiatry 89:1024–1031
39. Lanata SC, Miller BL (2016) The behavioural variant frontotemporal dementia (bvFTD) syndrome in psychiatry. J Neurol Neurosurg Psychiatry 87:501–511